Applications and Applied Mathematics: An International Journal (AAM)

Volume 16 | Issue 1 | Article 36

6-2021

Significance of Coriolis Force on Eyring-Powell Flow Over A Rotating Non-uniform Surface

Abayomi S. Oke
Kenyatta University

Winifred N. Mutuku
Kenyatta University

Follow this and additional works at: https://digitalcommons.pvamu.edu/aam

Part of the Applied Mathematics Commons

Recommended Citation

Oke, Abayomi S. and Mutuku, Winifred N. (2021). Significance of Coriolis Force on Eyring-Powell Flow Over A Rotating Non-uniform Surface, Applications and Applied Mathematics: An International Journal (AAM), Vol. 16, Iss. 1, Article 36.
Available at: https://digitalcommons.pvamu.edu/aam/vol16/iss1/36

This Article is brought to you for free and open access by Digital Commons @PVAMU. It has been accepted for inclusion in Applications and Applied Mathematics: An International Journal (AAM) by an authorized editor of Digital Commons @PVAMU. For more information, please contact hvkoshy@pvamu.edu.

Available at
http://pvamu.edu/aam
Appl. Appl. Math.
ISSN: 1932-9466
Vol. 16, Issue 1 (June 2021), pp. 643–661

Applications and Applied Mathematics:
An International Journal
(AAM)

Significance of Coriolis Force on Eyring-Powell Flow Over A Rotating Non-uniform Surface

[1]Abayomi Samuel Oke and [2]Winifred Nduku Mutuku

Department of Mathematics and Actuarial Science
Kenyatta University
Nairobi, Kenya
[1]okeabayomisamuel@gmail.com; [2]mutukuwinnie@gmail.com

Received: July 7, 2020; Accepted: December 17, 2020

Abstract

Coriolis force plays significant roles in natural phenomena such as atmospheric dynamics, weather patterns, etc. Meanwhile, to circumvent the unreliability of Newtonian law for flows involving varying speed, Eyring-Powell fluid equations are used in computational fluid dynamics. This paper unravels the significance of Coriolis force on Eyring-Powell fluid over the rotating upper horizontal surface of a paraboloid of revolution. Relevant body forces are included in the Navier-Stokes equations to model the flow of non-Newtonian Eyring-Powell fluid under the influence of Coriolis force. Using similarity transformation, the governing equations are nondimensionalized, thereby transforming the nonlinear partial differential equations to a system of boundary value nonlinear ordinary differential equations. The shooting technique is adopted to convert the boundary value problem to an initial value problem, which is in turn solved using the Runge-Kutta-Gill Scheme. At low Coriolis force, temperature profiles increase as Eyring-Powell parameter increases, whereas at high Coriolis force, temperature profiles decrease with increasing Eyring-Powell parameter.

Keywords: Coriolis Force; Eyring-Powell; Non-uniform surface; Upper horizontal surface of a paraboloid of revolution; Rotating surface; Non-Newtonian fluid

MSC 2010 No.: 76F10, 76A05, 76U05, 76N20, 76A02

1. Introduction

A fluid deforms continuously when shear stress is applied (Kaur et al. (2020); Urbina et al. (2020); Dessie and Fissha (2020); Choudhury and Ahmed (2018); Abualnaja (2018)). When shear stress (not up to the yield strength) is applied on a fluid and then removed, the fluid is expected to retract to its original form, retaining its properties. In the case that the shear stress is applied for a long time, the fluid may deform permanently. This tendency of a fluid to deform permanently is called creep. It is clear that exposing a fluid to high stress, just below its yield strength, can lead to creep. Creep occurs in paints, clay slips, cellulose derivatives, greases, etc. This kind of flow can be modeled to involve breaking two types of bond: a strong bond and a weak bond. The strong bond obeys the exponential law while the weak bond obeys the weak law. These fluids can be modeled as the Eyring-Powell fluid whose stress tensor τ is defined by the hyperbolic-sine law (Kubat and Rigdahl (1976); Linz and Dohle (1999); Powell and Eyring (1944); Urbina et al. (2020); Xu (2016); Yoon and Ghajar (1987)). Importance of Eyring-Powell fluids in physical substances includes the formation of fog, thermal insulation and underground energy transport (Babu et al. (2016); Nadeem et al. (2012); Malik et al. (2013); Mamun et al. (2016); Patel and Timol (2009); Rahimi et al. (2017); Sirohi et al. (1987)). Research carried out on Eyring-Powell fluid includes a three-dimensional flow of Eyring-Powell fluid, magnetohydrodynamic flow of Eyring-Powell, buoyancy-induced flow of Eyring-Powell fluid over different surfaces such as a plane horizontal surface, a stretching surface, inclined planes, etc. In most of the cases, it was recorded that Eyring-Powell parameter and buoyancy have a positive effect on the flow velocity but temperature responds negatively to buoyancy (Abualnaja (2018); Choudhury and Ahmed (2018); Dessie and Fissha (2020); Mushtaq et al. (2013); Agbaje et al. (2016); Koriko et al. (2017); Jafarimoghaddam (2019); Nawaz et al. (2019); Umar et al. (2019); Alsaedi et al. (2020); Kumar and Srinivas (2020); Waqas et al. (2020); Hayat et al. (2013); Javed et al. (2013); Siddiqui et al. (2014); Babu et al. (2016)). One work that contradicts most of the existing results is that of Abegunrin et al. (Abegunrin et al. (2017)) where Blasius flow of Eyring-Powell fluid over a non-uniform surface is considered. Abegunrin et al. recorded that the overall flow velocity decreases with Eyring-Powell parameter.

Coriolis force is the fictitious force responsible for the deflection of the trajectory of an object moving in a rotating frame of reference. Coriolis effect has been found to be significant in many physical and natural situations. Coriolis effect is the only perfect explanation for the changes in weather patterns, the direction of cyclonic storms, the arrangement of Earth's magnetic and electric currents in columns, etc. More so, many of the physical surfaces in nature and application are neither a horizontal plane nor a vertical plane but parabolic in nature. In order to generalize these surfaces, Animasaun (2016) introduced the upper horizontal surface of a paraboloid of revolution (*uhspr.*) which generalizes surfaces with uniform thickness (such as, the horizontal plane, vertical plane, inclined plane) and surfaces with a non-uniform thickness (such as the outer surface of a bullet, the Earth's surface, etc.). Since the proposal of this surface, several authors have carried out researches to unravel flows over surface with non-uniform surfaces (Animasaun (2016); Animasaun (2018); Hudson et al. (1978); Hussain et al. (2017); Kaur et al. (2020); Khasawneh et al. (2009); Koriko et al. (2020b); Kumar (2018); Lee et al. (2017); Liang and Chan (2005);

Makinde and Animasaun (2016); Malik et al. (2013); Mamun et al. (2016); Mitteilungen (1972); Zin et al. (2017); Zhavoronkov et al. (1978)).

To the best of our knowledge, the flow of Eyring-Powell fluid over a rotating non-uniform surface has not been investigated. Motivated by this fact, we investigate the flow of Eyring-Powell fluid over a surface that is neither a horizontal nor a vertical nor a perfectly inclined plane is studied while taking the influence of Coriolis force into consideration. The flow configuration and the governing equations with the similarity variables and the dimensionless equations are presented in Section 2. The equations are solved numerically and the simultaneous effects of Eyring-Powell parameter, buoyancy, deformation parameter with Coriolis force are investigated. The graphs are discussed in Section 4.

2. Formulation of Governing Equations

A two-dimensional Eyring-Powell fluid flow is considered in this study. The fluid and the heated surface are assumed to be in rigid body rotation at uniform angular velocity $\boldsymbol{\Omega}$. The flow configuration is shown in Figure 1. The fluid flows over the region $y \geq 0$. As a result of the angular velocity $\boldsymbol{\Omega}$, the system produces Coriolis force $2\boldsymbol{\Omega} \times \boldsymbol{V}$, where the velocity $\boldsymbol{V}$ of the fluid is $\boldsymbol{V} = (u, v, w)$. The stress tensor τ is defined by the hyperbolic-sine law

$$\tau = \mu \nabla \overrightarrow{v} + \frac{1}{B} \sinh^{-1}\left(\frac{1}{C} \nabla \overrightarrow{v}\right), \tag{1}$$

where the second term is responsible for the deformation of the fluid. Using the body forces proposed by Koriko et al. (2020b) and Koriko et al. (2020a) and validate by Oke et al. (2020b) and Oke et al. (2020a), the continuity, momentum and energy equations for a two dimensional Eyring-Powell fluid are

$$\frac{\partial u}{\partial x} + \frac{\partial v}{\partial y} = 0, \tag{2}$$

$$\begin{aligned} u\frac{\partial u}{\partial x} + v\frac{\partial u}{\partial y} + 2\frac{\Omega \aleph w}{U_0(x+b)^{2-m}} =& \frac{\mu}{\rho}\frac{\partial^2 u}{\partial y^2} + \left(\frac{m+1}{2}\right) g\beta\left(T - T_\infty\right) \\ &+ \frac{1}{\rho B C}\left(1 - \frac{1}{2C^2}\left(\frac{\partial u}{\partial y}\right)^2\right)\frac{\partial^2 u}{\partial y^2} - \frac{1}{\rho}\frac{\partial p}{\partial x}, \end{aligned} \tag{3}$$

$$\begin{aligned} u\frac{\partial w}{\partial x} + v\frac{\partial w}{\partial y} - 2\frac{\Omega \aleph u}{U_0(x+b)^{2-m}} =& \frac{\mu}{\rho}\frac{\partial^2 w}{\partial y^2} + \left(\frac{m+1}{2}\right) g\beta\left(T - T_\infty\right) \\ &+ \frac{1}{\rho B C}\left(1 - \frac{1}{2C^2}\left(\frac{\partial w}{\partial y}\right)^2\right)\frac{\partial^2 w}{\partial y^2} - \frac{1}{\rho}\frac{\partial p}{\partial x}, \end{aligned} \tag{4}$$

$$u\frac{\partial T}{\partial x} + v\frac{\partial T}{\partial y} = \frac{\kappa}{\rho c_P}\frac{\partial^2 T}{\partial y^2}, \tag{5}$$

subject to the boundary conditions

$$\text{at } y = A\left(x+b\right)^{\frac{1-m}{2}} : \; u = U_0\left(x+b\right)^m, \; v = 0, \; w = 0, \; T = T_w, \tag{6}$$

$$\text{as } y \to \infty : u \to 0, \; w \to 0, \; T \to T_\infty, \tag{7}$$

where μ is the coefficient of viscosity, ρ is the fluid density, g is the acceleration due to gravity, β is the coefficient of thermal expansion, T is the temperature of the fluid, c_p is the specific heat capacity, κ is the thermal conductivity and $T_w = A\,(x+b)^{\frac{1-m}{2}}$. The Bernoulli equation for the free stream flow of a boundary layer where there is no viscosity is given as

$$\frac{p}{\rho} + \frac{U_e^2}{2} = \text{constant} \;\Rightarrow\; \frac{\partial}{\partial x}\left(\frac{p}{\rho} + \frac{U_e^2}{2}\right) = 0 \;\Rightarrow\; -\frac{1}{\rho}\frac{\partial p}{\partial x} = 0.$$

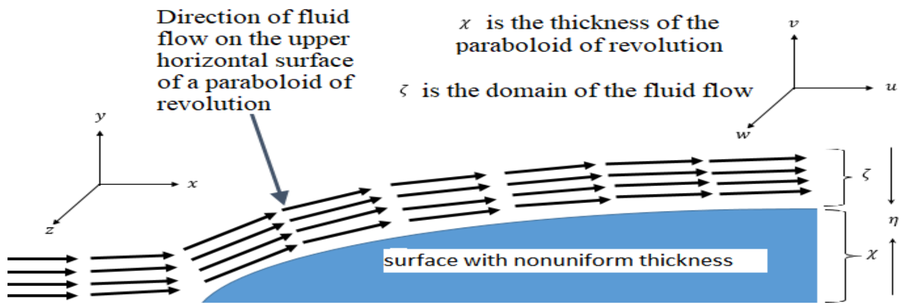

Figure 1. Flow configuration

The governing equations are rendered dimensionless by using the similarity variables

$$u = \frac{\partial \psi}{\partial y},\; v = -\frac{\partial \psi}{\partial x},\; w\,(\eta) = U_0\,(x+b)^m\, h(\eta),\; \theta = \frac{T - T_\infty}{T_w - T_\infty}, \tag{8}$$

$$\psi = \left(\frac{2}{m+1}\right)^{\frac{1}{2}} (\nu U_0)^{\frac{1}{2}}\,(x+b)^{\frac{m+1}{2}}\, f(\eta), \eta = y\left(\frac{m+1}{2}\frac{U_0}{\nu}\right)^{\frac{1}{2}} (x+b)^{\frac{m-1}{2}}, \tag{9}$$

and the nondimensionalized equations become

$$\left(1 + \epsilon - \epsilon\delta\left(\frac{m+1}{2}\right) f''^2\right) f''' - \frac{2m}{m+1} f'^2 + f'' f - \frac{K}{(m+1)} h + Gr\theta = 0, \tag{10}$$

$$\left(1 + \epsilon - \epsilon\delta\left(\frac{m+1}{2}\right) h'^2\right) h'' - \frac{2m}{m+1} h f' + h' f + \frac{K}{(m+1)} f' + Gr\theta = 0, \tag{11}$$

$$\theta'' + Pr f\theta' - Pr\left(\frac{1-m}{m+1}\right) f'\theta = 0, \tag{12}$$

with the boundary conditions

$$\text{at } \eta = \chi: \quad f' = 1,\; f = \left(\frac{1-m}{m+1}\right)\chi,\; h = 0,\; \theta = 1, \tag{13}$$

$$\text{as } \eta \to \infty: f' \to 0,\; h \to 0,\; \theta \to 0, \tag{14}$$

where

$$\epsilon = \frac{1}{\mu BC}, \ \delta = \frac{U_0^3}{2\nu C^2}(x+b)^{(3m-1)}, \tag{15}$$

$$K = \frac{4\Omega}{U_0^2(x+b)}, \ Gr = \frac{g\beta(T_w - T_\infty)}{U_0^2(x+b)^{2m-1}}, \tag{16}$$

$$Pr = \frac{\rho c_P \nu}{\kappa}, \quad \chi = A\left(\frac{m+1}{2}\frac{U_0}{\nu}\right)^{\frac{1}{2}} \tag{17}$$

K is the rotational parameter, Gr is Grashof number, Pr is Prandtl number, χ is the thickness parameter, m is the surface non-uniformity index and ϵ, and δ are the Eyring-Powell parameters. The quantities of practical interest are the coefficients of skin friction along the $x-$ and $z-$directions and the heat transfer rate and they are defined respectively as

$$Re_x^{\frac{1}{2}} C_{fx} = F''(0),$$
$$Re_x^{\frac{1}{2}} C_{fz} = H'(0),$$
$$Re_x^{-\frac{1}{2}} N_{ux} = -\Theta'(0).$$

3. Numerical Solution

Analytical approach, semi-analytical approach and numerical approach are the three methods adopted for solving differential equations (Oke (2017)). However, analytical methods are not always feasible due to the non-linearity of models generated from physical and industrial applications; this makes semi-analytical and numerical approaches the most viable tools. In this study, a numerical approach is adopted to unravel the dynamics of the flow under consideration. The Runge-Kutta Gill Formula is used. This scheme involves using the fourth-order Runge Kutta method alongside some constants introduced by Gill. The method is described for an ordinary differential equation of the form

$$y' = f(y), \ y(t_0) = y_0,$$

as

$$k_1 = hf(y_n), \ k_2 = hf\left(y_n + \frac{1}{2}k_1\right),$$
$$k_3 = hf(y_n + ak_1 + bk_2), \ k_4 = hf(y_n + ck_2 + dk_3),$$
$$y_{n+1} = y_n + \frac{1}{6}(k_1 + 2bk_2 + 2dk_3 + k_4),$$

where

$$a = \frac{\sqrt{2}-1}{2}, \ b = \frac{2-\sqrt{2}}{2}, \ c = \frac{\sqrt{2}}{2}, \ d = \frac{\sqrt{2}+2}{2},$$

which is stable for $h \leq (2.8/\lambda)$. As $\epsilon \to 0$ and $\delta \to 0$, the flow reduces to the one considered in (Koriko et al. (2020b)). The results of this study is validated by comparing with the results of Koriko et al. (2020b) and the comparison is shown in Table 1.

Table 1. Validation of results for coefficients of friction and heat transfer coefficients

K	$f''(0)$ Present	$f''(0)$ (Koriko et al. (2020b))	$h'(0)$ Present	$h'(0)$ (Koriko et al. (2020b))	$-\theta'(0)$ Present	$-\theta'(0)$ (Koriko et al. (2020b))
0	-0.314749068	-0.314749068	0.615690322	0.615690322	3.439015982	3.439015982
0.1	-0.320716879	-0.320716880	0.672570086	0.672570086	3.437631190	3.437631200
0.2	-0.329661029	-0.329661030	0.729005666	0.729005666	3.435503462	3.435503462
0.3	-0.341459563	-0.341459563	0.784465936	0.784465933	3.432658578	3.432658578
0.4	-0.355891566	-0.355891570	0.838434304	0.838434301	3.429141050	3.429141050
0.5	-0.372633523	-0.372633523	0.890450675	0.890450673	3.425020944	3.425020944

4. Results and Discussion

Equations governing the flow of Eyring-Powell fluid over a rotating non-uniform surface are formulated as partial differential equations in Equation 2 through Equation 5 and the similarity variables in equation 8 through Equation 9 are used to render them dimensionless as the ordinary differential equations in Equation 10 through Equation 12. Since the analytical solution of the governing equations is difficult to obtain (Oke (2017)), the dynamics of the flow as Coriolis force increases from low to moderately high is studied by numerically solving Equation 10 through Equation 12 using Runge-Kutta-Gills method alongside Shooting Technique and the results are illustrated as graphs. Specifically, the effects of Grashof number Gr (i.e. buoyancy), velocity index m (surface non-uniformity index), Eyring-Powell parameter ϵ (rate of fluid deformation) and Prandtl number Pr (ratio of momentum diffusivity to thermal diffusivity) as Coriolis effect increases are analyzed.

The effects of Coriolis force is measured by increasing the rotational parameter K which is proportional to the Coriolis force. By fixing all flow conditions such that $Gr = 5$, $Pr = 2.0$, $m = 0.3$, $\epsilon = 0.1$, $\delta = 0.1$, and $\chi = 0.25$, the effects of Coriolis force on the flow are studied. The counterclockwise rotation of the surface (as shown in Figure 1) reduces the kinetic energy of the fluid parcels flow in the $x-$direction and increases the kinetic energy of the fluid parcels in the positive $z-$direction. The variation in the kinetic energy causes the velocity profile in the $x-$direction to reduce as Coriolis force increases (as illustrated in Figure 2) and the velocity profile in the $z-$direction to increase as Coriolis force increases (as illustrated in Figure 3). More energy is added to the system as Coriolis force increase as a consequence of the rotation, thereby raising the temperature profiles as Coriolis force increases (see Figure 4 and the zoomed portion in 5). It is important to mention that the rotation parameter cannot exceed a certain value (which in this case is 0.5), otherwise the flow becomes turbulent and the Coriolis effects become difficult to measure. It appears that there are periodic solutions at $0.5 < K < 1.0$ and no unique solution at $K > 1.0$.

The Grashof number measures buoyancy effect on the flow. In this study, buoyancy effect is measured on the flow by setting $Pr = 2.0$, $m = 0.3$, $\epsilon = 0.1$, $\delta = 0.1$, and $\chi = 0.25$ and increasing the Grashof number. Buoyancy converts the heat energy to internal kinetic energy for the fluid particles. It is therefore expected that the velocity profiles in both directions are enhanced and this is supported by Figure 6 and Figure 7 where the velocity profiles in $x-$ and $z-$directions respectively increase as Grashof number increases. As a result of this, as Coriolis force increases alongside Grashof number, the effect of Grashof number is impeded on velocity profiles in the $x-$direction but enhanced on velocity profiles in the $z-$direction. Hence, it is valid to ascertain that the maximum velocity profile in the $x-$direction is obtained at high Grashof number but low Coriolis force. More so, the maximum velocity profile in the $z-$direction is obtained at high Grashof number and high Coriolis force. More so, it is clear that heat energy is converted causing a reduction in temperature profiles as observed in Figure 8. It is also observed from Figure 8 that increasing Coriolis force impedes the decreasing effect of Grashof number on the temperature profiles, hence maximum temperature profile is obtained at high Coriolis force but low Grashof number.

A continuous increase of the surface non-uniformity index m from 0 to 1 gradually changes the surface from the upper horizontal surface of a paraboloid of revolution to a flat sheet. To study the effect of the surface non-uniformity index m, other parameters are set as $Gr = 5$, $Pr = 2.0$, $\epsilon = 0.1$, $\delta = 0.1$, and $\chi = 0.25$. It is worth mentioning that as m increases from 0 to 1, the non-uniformity is gradually removed and the required energy for climbing the non-uniformity reduces. The system does less work and the fluid flow is enhanced in all direction. Figure 9 and Figure 10 show that the velocity profiles in the $x-$ and $z-$directions increase respectively as the surface non-uniformity index m increases. It is also observed that increasing Coriolis force counters the effect of increasing surface non-uniformity index m on the velocity profiles in the $x-$direction (see Figure 9), hence maximum velocity profile in the $x-$direction is obtained on a slowly rotating uniform surface but maximum velocity profile in the $z-$direction is obtained on a moderately fast-rotating uniform surface. Meanwhile, increasing Coriolis force magnifies the effect of increasing surface non-uniformity index m on the velocity profiles in the $z-$direction (see (10)). Figure 11 shows that the temperature profile also increases with increasing surface non-uniformity index m. It is remarked here that the maximum temperature profile is obtained on a moderately fast-rotating uniform surface.

The Eyring-Powell parameter ϵ measures the rate of deformation of the fluid and the fluid becomes Newtonian as $\epsilon \to 0$. It is worthwhile to note that shear thinning occurs with the increase in the value of ϵ. From Figure 12, it is revealed that velocity profiles in the $x-$direction increases as Eyring-Powell parameter ϵ increases. A shown in Figure 13, as Eyring-Powell parameter ϵ increases, velocity profiles in the $z-$direction decreases within the boundary layer but increases at the free stream. It is valid to remark that the minimum velocity profile in the $x-$direction occurs as $\epsilon \to 0$ (i.e., Newtonian flow) at high Coriolis force and the maximum velocity profile in the $z-$direction occurs as $\epsilon \to 0$ (i.e Newtonian flow) at high Coriolis force. It can be seen from Figure 14 (the zoomed portion is shown in Figure 15) that the temperature profiles respond to increasing Eyring-Powell parameter ϵ differently at different Coriolis force. At low Coriolis force, temperature profiles increase as Eyring-Powell parameter ϵ increases whereas at high Coriolis force, temperature profiles decrease with increasing Eyring-Powell parameter ϵ.

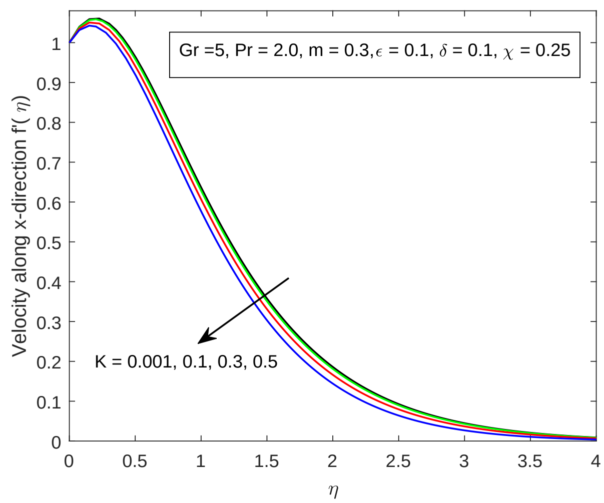

Figure 2. Effect of increasing Coriolis force on the velocity profile in the $x-$direction

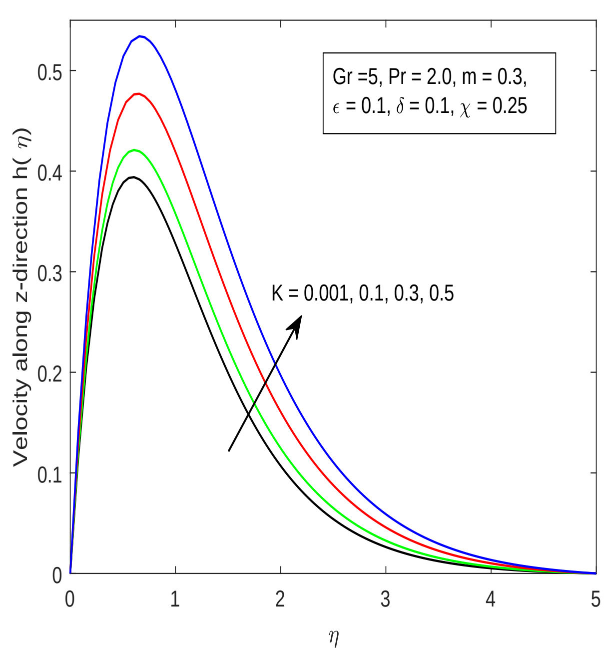

Figure 3. Effect of increasing Coriolis force on the velocity profile in the $z-$direction

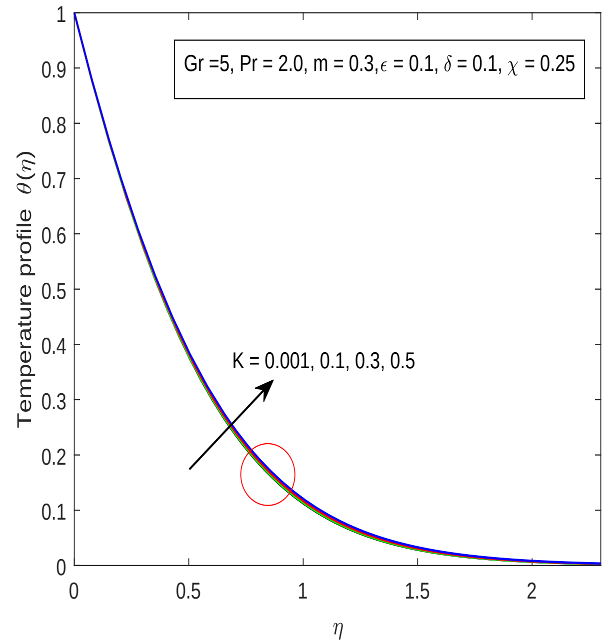

Figure 4. Effect of increasing Coriolis force on the temperature profile

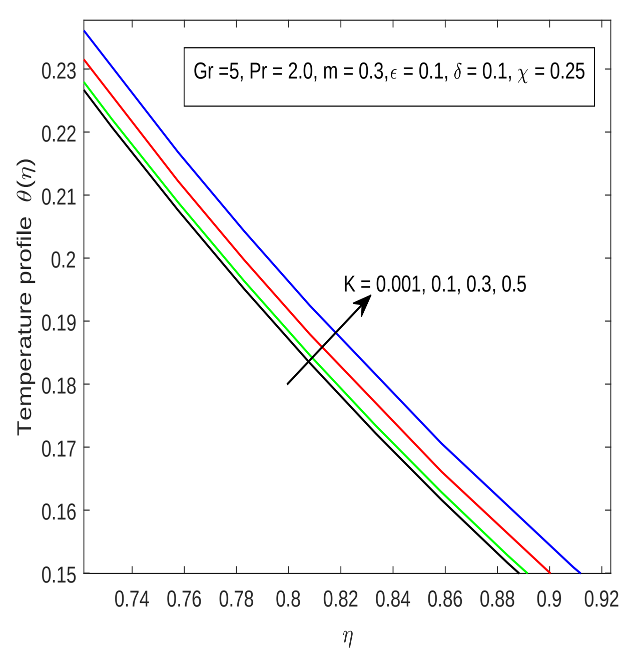

Figure 5. Zoomed portion of Figure 4

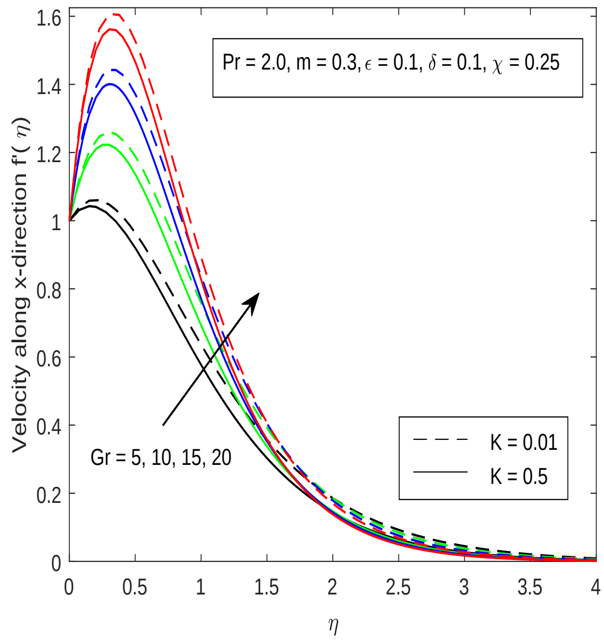

Figure 6. Effect of Grashof number Gr on velocity profiles in the $x-$direction at low and large Coriolis force

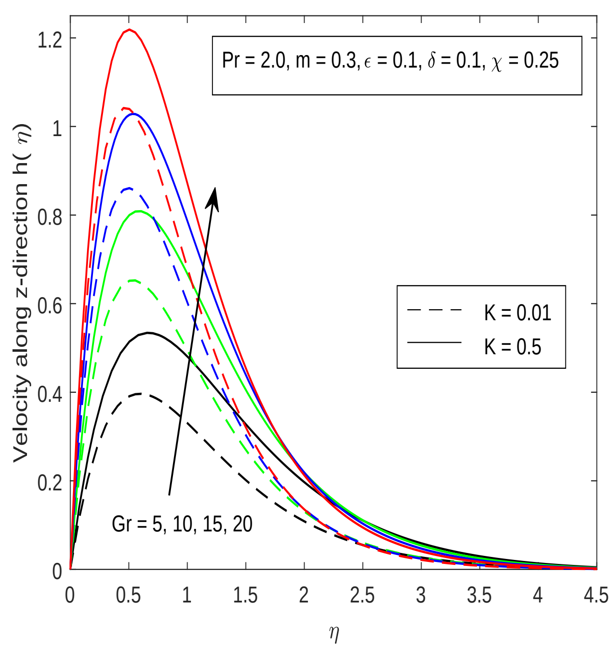

Figure 7. Effect of Grashof number Gr on velocity profiles in the $z-$direction at low and large Coriolis force

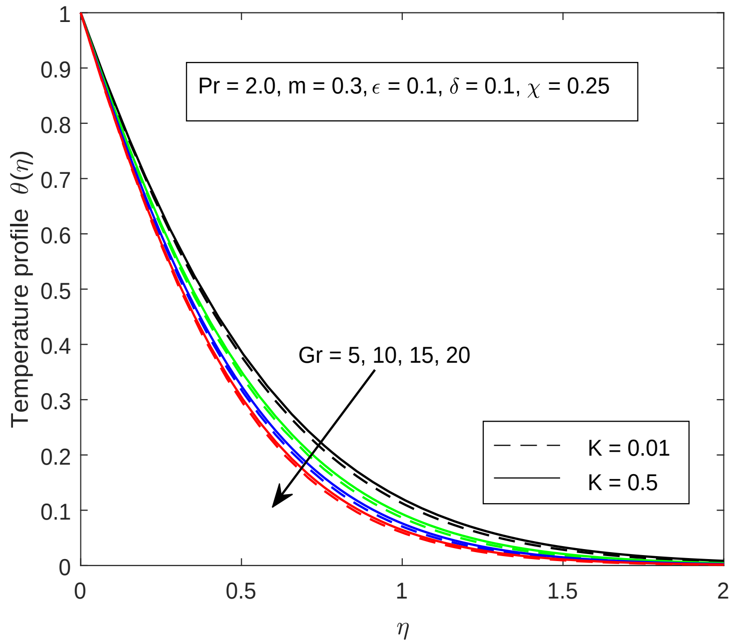

Figure 8. Effect of Grashof number Gr on temperature profiles at low and large Coriolis force

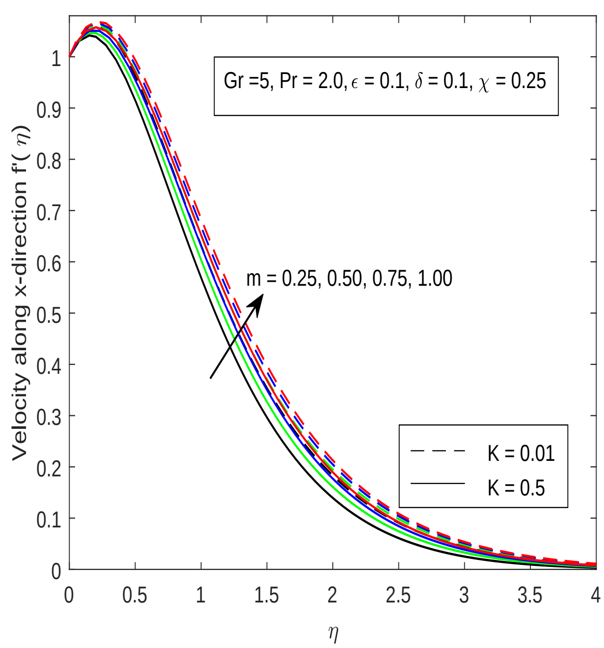

Figure 9. Effect of velocity index m on velocity profiles in the $x-$direction at low and large Coriolis force

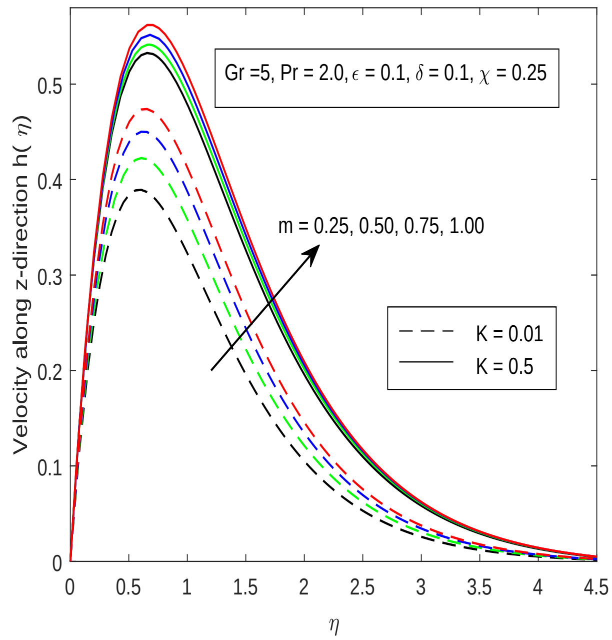

Figure 10. Effect of velocity index m on velocity profiles in the $z-$direction at low and large Coriolis force

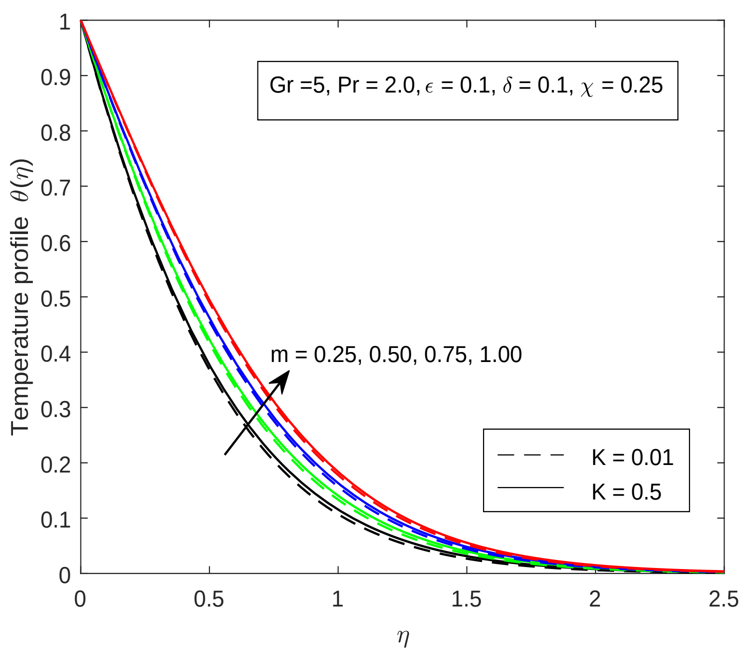

Figure 11. Effect of velocity index m on temperature profiles at low and large Coriolis force

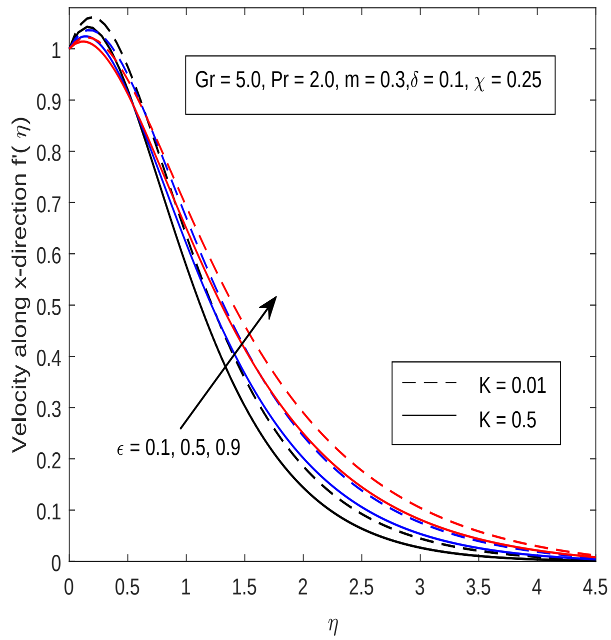

Figure 12. Effect of Eyring-Powell parameter ϵ on velocity profiles in the $x-$direction at low and large Coriolis force

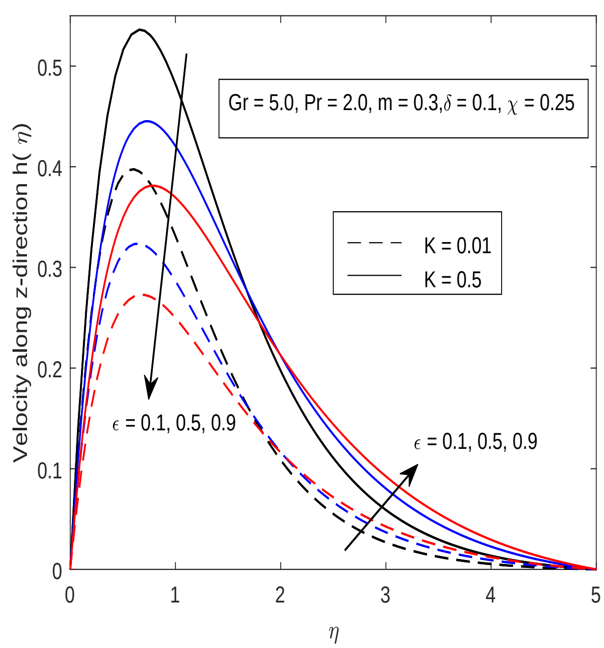

Figure 13. Effect of Eyring-Powell parameter ϵ on velocity profiles in the $z-$direction at low and large Coriolis force

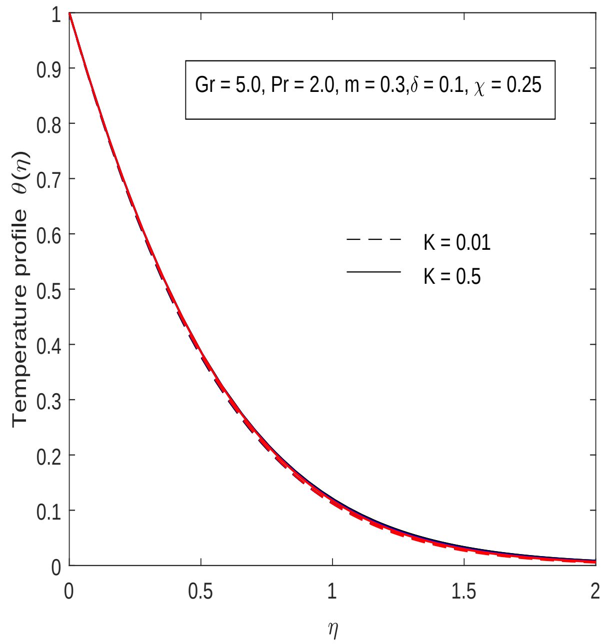

Figure 14. Effect of Eyring-Powell parameter ϵ on temperature profiles at low and large Coriolis force

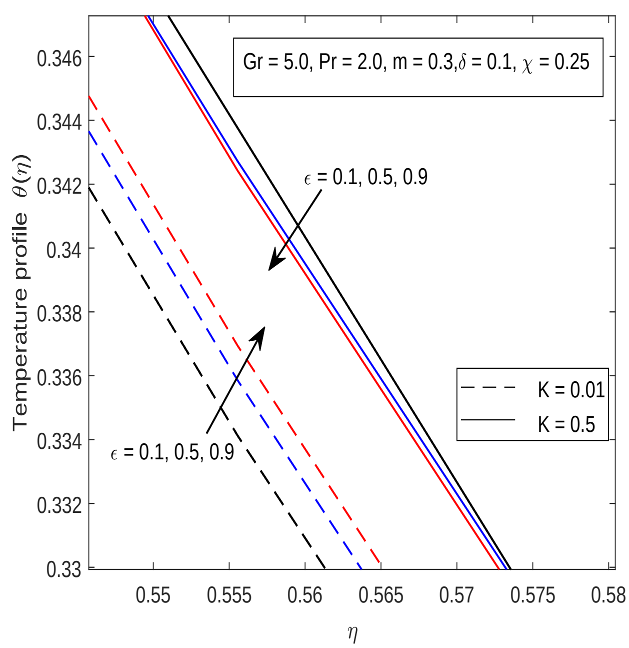

Figure 15. Zoomed portion of Figure 14

As shown in Table 2, the coefficient of skin friction in both $x-$ and $z-$directions and the heat transfer rate decrease with increasing Eyring-Powell parameter and increase in the Coriolis force causes a further decrease. It can be seen from Table 3 that increase in Grashof number causes an increase in the coefficient of skin friction in both $x-$ and $z-$direction and the heat transfer rate. Meanwhile, as Coriolis force increases, the coefficient of skin friction in $z-$direction and the heat transfer rate decreases while the coefficient of skin friction in both $x-$direction and the heat transfer rate increase the more. The effect of Coriolis force on the coefficient of skin friction in both $x-$ and $z-$direction and the heat transfer rate when all other parameters are fixed is shown in Table 4. It is clear that increase in rotation leads to a decrease in the coefficient of skin friction in both $x-$direction and the heat transfer rate but an increase in the coefficient of skin friction in the $z-$direction.

Table 2. Variation of quantities of interest with Eyring-Powell parameter ϵ at low and at high rotation

K	Gr	m	ϵ	C_{fx}	C_{fz}	N_{ux}
0.01	5.0	0.3	0.1	0.6787	1.7097	1.6562
0.01	5.0	0.3	0.5	0.4508	1.3257	1.6468
0.01	5.0	0.3	0.9	0.3147	1.0685	1.6410
0.50	5.0	0.3	0.1	0.5687	2.0801	1.6334
0.50	5.0	0.3	0.5	0.3692	1.6398	1.6291
0.50	5.0	0.3	0.9	0.2517	1.3260	1.6269

Table 3. Variation of quantities of interest with Grashof number Gr at low and at high rotation

K	m	ϵ	Gr	C_{fx}	C_{fz}	N_{ux}
0.01	0.3	0.1	5	0.6772	1.6912	1.6562
0.01	0.3	0.1	10	1.9702	3.1026	1.7703
0.01	0.3	0.1	15	3.1796	4.4358	1.8574
0.01	0.3	0.1	20	4.3613	5.768	1.9299
0.5	0.3	0.1	5	0.5682	2.0465	1.6334
0.5	0.3	0.1	10	1.8313	3.5422	1.7476
0.5	0.3	0.1	15	3.0171	4.9572	1.8352
0.5	0.3	0.1	20	4.1752	6.3879	1.9082

Table 4. Variation of quantities of interest with Coriolis force

K	χ	C_{fx}	C_{fz}	N_{ux}
0.001	0.25	0.6786	1.6848	1.6564
0.1	0.25	0.6621	1.7559	1.6532
0.3	0.25	0.6206	1.901	1.6447
0.5	0.25	0.5682	2.0465	1.6334

5. Conclusion

The flow of Eyring-Powell non-Newtonian fluid over a rotating non-uniform surface is studied and the combined effect of the pertinent parameters and Coriolis force are investigated. The outcomes are listed below.

(1) Effects of increasing Coriolis force under constant conditions are:
  - reduction in velocity profiles in the $x-$direction.
  - increase in velocity profiles in the $z-$direction.

(2) Effects of simultaneous increase in both Grashof number and Coriolis force are:
  - the maximum velocity profile in the $x-$direction is obtained at high Grashof number but low Coriolis force.
  - the maximum velocity profile in the $z-$direction is obtained at high Grashof number and high Coriolis force.
  - the maximum temperature profile is obtained at high Coriolis force but low Grashof number.

(3) As the surface becomes more uniform:
  (a) the maximum velocity profile in the $x-$direction is obtained on a slowly rotating uniform surface
  (b) the maximum velocity profile in the $z-$direction is obtained on a moderately fast rotating uniform surface.
  (c) the maximum temperature profile is obtained on a moderately fast rotating uniform surface.

(4) Effects of Eyring-Powell parameter are:
  (a) the minimum velocity profile in the $x-$direction occurs for a Newtonian flow at high Coriolis force
  (b) the maximum velocity profile in the $z-$direction occurs for a Newtonian flow at high Coriolis force.
  (c) at low Coriolis force, temperature profiles increase as Eyring-Powell parameter ϵ increases whereas at high Coriolis force, temperature profiles decrease with increasing Eyring-Powell parameter ϵ.

REFERENCES

Abegunrin, O. A., Animasaun, I. L. and Sandeep, N. (2017). Insight into the boundary layer flow of non-Newtonian Eyring-Powell fluid due to catalytic surface reaction on an upper horizontal surface of a paraboloid of revolution, Alexandria Engineering Journal, pages 1–10.

Abualnaja, K. M. (2018). Numerical studies for MHD flow and gradient heat transport past a stretching sheet with radiation and heat production via DTM, Vol. 13, No. 2, pp. 915-924.

Agbaje, T. M., Mondal, S., Motsa, S. S. and Sibanda, P. (2016). A numerical study of unsteady non-Newtonian Powell-Eyring nanofluid flow over a shrinking sheet with heat generation and thermal radiation, Alexandria Engineering Journal, pages 1–11.

Alsaedi, A., Hayat, T., Qayyum, S. and Yaqoob, R. (2020). Eyring-Powell nanofluid flow with nonlinear mixed convection: Entropy generation minimization, Computer Methods and Programs in Biomedicine, Vol. 186, 105183.

Animasaun, I. L. (2016). 47nm alumina-water nanofluid flow within boundary layer formed on upper horizontal surface of paraboloid of revolution in the presence of quartic autocatalysis chemical reaction, Alexandria Engineering Journal, Vol. 55, No. 3, pp. 2375–2389.

Animasaun, I. L. (2018). Quartic autocatalytic chemical reaction in boundary layer flow over upper horizontal surface of a paraboloid of revolution, PhD thesis, Federal University of Technology, Akure, Ondo State, Nigeria.

Babu, M. J., Sandeep, N. and Raju, C. S. (2016). Heat and mass transfer in MHD Eyring-Powell nanofluid flow due to cone in porous medium, International Journal of Engineering Research in Africa, Vol. 19, pp. 57–74.

Choudhury, K. and Ahmed, N. (2018). Soret effect on transient MHD convective flow past a aemi-infinite vertical porous plate with heat sink and chemical reaction, Appl. Appl. Math., Vol. 13, No. 2, pp. 839-853.

Dessie, H. and Fissha, D. (2020). MHD mixed convective flow of Maxwell nanofluid past a porous vertical stretching sheet in presence of chemical reaction, Appl. Appl. Math., Vol. 15, No. 1, pp. 530-549.

Hayat, T., Awais, M. and Asghar, S. (2013). Radiative effects in a three-dimensional flow of MHD Eyring-Powell fluid, Journal of the Egyptian Mathematical Society, Vol. 21, pp. 379–384.

Hudson, J. L., Tang, D. and Abell, S. (1978). Experiments on centrifugally driven thermal convection in a rotating cylinder, J . Fluid Mech., Vol. 86, No. 1, pp. 147–159.

Hussain, S., Jain, J., Seth, G.S. and Rashidi, M.M. (2017). Free convective heat transfer with hall effects, heat absorption and chemical reaction over an accelerated moving plate in a rotating system, Journal of Magnetism and Magnetic Materials, Vol. 422, pp. 112–123.

Jafarimoghaddam, A. (2019). Mhd flow of Eyring-Powell fluids: HPM and a novel topological technique, Heat Transfer Asian Research, Vol. 48, No. 3, pp. 982–1001.

Javed, T., Ali, N., Abbas, Z. and Sajid, M. (2013). Flow of an Eyring-Powell non-Newtonian fluid over a stretching sheet, Chem. Eng. Comm., Vol. 200, pp. 327–336.

Kaur, B., Kumar, D. and Chauhan, S. (2020). A study of small perturbations in the Coriolis and centrifugal forces in RR3BP with finite straight segment, Appl. Appl. Math., Vol. 15, No. 1, pp. 77-93.

Khasawneh, K., Dababneh, S. and Odibat, Z. (2009). A solution of the neutron diffusion equation in hemispherical symmetry using the homotopy perturbation method, Annals of Nuclear Energy, Vol. 36, pp. 1711–1717.

Koriko, O. K., Adegbie, K. S., Oke, A. S. and Animasaun, I. L. (2020a). Corrigendum: Exploration of Coriolis force on motion of air over the upper horizontal surface of a paraboloid of revolution, Phys. Scr., Vol. 95, 035210.

Koriko, O. K., Adegbie, K. S., Oke, A. S. and Animasaun, I. L. (2020b). Exploration of Coriolis force on motion of air over the upper horizontal surface of a paraboloid of revolution, Physica Scripta, IOP Publishing, Vol. 95, 035210.

Koriko, O. K., Animasaun, I. L., Reddy, M. G. and Sandeep, N. (2017). Scrutinization of thermal stratification, nonlinear thermal radiation and quartic autocatalytic chemical reaction effects on the flow of three-dimensional Eyring-Powell alumina-water nanofluid, Multidiscipline Modeling in Materials and Structures.

Kubat, J. and Rigdahl, M. (1976). The exponential and power laws of stress relaxation kinetics and a general relation between the activation volume and effective stress, The Laws of Stress Relaxation Kinetics Phys. Stat. Sol., Vol. 35, pp. 173–180.

Kumar, B. and Srinivas, S. (2020). Unsteady hydromagnetic flow of Eyring-Powell nanofluid over an inclined permeable stretching sheet with Joule heating and thermal radiation, Journal of Applied and Computational Mechanics, Vol. 6, No. 2, pp. 259–270.

Kumar, R. (2018). Numerical exploration of thermal radiation and rotation effects on the 3-dimensional flow of cu-water nanofluid over an oscillating flat surface, Int. J. Appl. Comput. Math, Vol. 9.

Lee, S., Ryi, S.-K. and Lim, H. (2017). Solutions of Navier-Stokes equation with Coriolis force, Advances in Mathematical Physics, 7042686.

Liang, X. and Chan, J. C. (2005). The effects of the full Coriolis force on the structure and motion of a tropical cyclone. Part I: Effects due to vertical motion, American Meteorological Society, Vol. 62, pp. 3825 - 3830.

Linz, S. J. and Dohle, A. (1999). Minimal relaxation law for compaction of tapped granular matter, Physical Review E, Vol. 60, No. 5, pp. 5737 - 5741.

Makinde, O. D. and Animasaun, I. L. (2016). Thermophoresis and Brownian motion effects on MHD bioconvection of nanofluid with nonlinear thermal radiation and quartic chemical reaction past an upper horizontal surface of a paraboloid of revolution, Journal of Molecular Liquids, Vol. 221, pp. 733 - 743.

Malik, M. Y., Hussain, A. and Nadeem, S. (2013). Boundary layer flow of an Eyring-Powell model fluid due to a stretching cylinder with variable viscosity, Scientia Iranica B, Vol. 20, No. 2, pp. 313-321.

Mamun, K., Rahman, M. M., Akhter, M. N., and Ali, M. (2016). Physiological non-Newtonian blood flow through single stenosed artery, International Conference on Mechanical Engineering, Vol. 1754, pp. 1–9.

Mitteilungen, K. (1972). On unsteady magnetohydrodynamic boundary layers in a rotating flow, ZAMM, Vol. 52, pp. 623 - 626.

Mushtaq, A., Mustafa, M., Hayat, T., Rahi, M. S., and Alsaedi, A. (2013). Exponentially stretching sheet in a Powell-Eyring fluid: Numerical and series solutions, Zeitschrift für Naturforschung A, Vol. 68, pp. 791 – 798.

Nadeem, S., Akbar, N. S. and Ali, M. (2012). Endoscopic effects on the peristaltic flow of an Eyring-Powell fluid, Meccanica, Vol. 47, No. 687–697.

Nawaz, M., Qureshi, I. H., and Shahzad, A. (2019). Thermal performance of partially ionized Eyring-Powell liquid: A theoretical approach, Physica Scripta, Vol. 94, No. 12, 125209.

Oke, A. S. (2017). Convergence of differential transform method for ordinary differential equations, Journal of Advances in Mathematics and Computer Science, Vol. 24, No. 6, pp. 1–17.

Oke, A. S., Mutuku, W. N., Kimathi, M. and Animasaun, I. L. (2020a) Coriolis effects on MHD newtonian flow over a rotating non-uniform surface, Proceedings of the Institution of Mechanical Engineers, Part C: Journal of Mechanical Engineering Science, Vol. 2020, 0954406220969730.

Oke, A. S., Mutuku, W. N., Kimathi, M. and Animasaun, I. L. (2020b) Insight into the dynamics of non-Newtonian Casson fluid over a rotating non-uniform surface subject to Coriolis force, Nonlinear Engineering, Vol. 2020, pp. 1-17.

Patel, M. and Timol, M. G. (2009). Numerical treatment of Powell-Eyring fluid flow using method of satisfaction of asymptotic boundary conditions (msabc), Applied Numerical Mathematics, Vol. 59, pp. 2584–2592.

Powell, R. E. and Eyring, H. (1944). Mechanisms for the relaxation theory of viscosity, Nature, Vol. 154, No. 3909, pp. 427–428.

Rahimi, J., Ganji, D. D., Khaki, M. and Hosseinzadeh, K. (2017). Solution of the boundary layer flow of an Eyring-Powell non-Newtonian fluid over a linear stretching sheet by collocation method, Alexandria Engineering Journal, pages 622–627.

Siddiqui, A. M., Haroon, T. and Zeb, M. (2014). Analysis of Eyring-Powell fluid in helical screw rheometer, The Scientific World Journal, Vol. 2014, pp. 1–14.

Sirohi, V., Timol, M. G. and Kalthia, N. L. (1987). Powell-Eyring model flow near an accelerated plate, Fluid Dynamics Research, Vol. 2, pp. 193–204.

Umar, M., Akhtar, R., Sabir, Z., Wahab, H.A., Zhiyu, Z., Imran, A., Shoaib, M. and Raja, M.A.Z. (2019). Numerical treatment for the three-dimensional Eyring-Powell fluid flow over a stretching sheet with velocity slip and activation energy, Advances in Mathematical Physics, Vol. 2019, pp. 1–12.

Urbina, G., Riahi, D. N. and Bhatta, D. (2020). Mathematical modeling of nonlinear blood glucose-insulin dynamics with beta cells effect, Appl. Appl. Math. Vol. 15, No. 1, pp. 171-191.

Waqas, M., Jabeen, S., Hayat, T., Shehzad, S. A. and Alsaedi, A. (2020). Numerical simulation for nonlinear radiated Eyring-Powell nanofluid considering magnetic dipole and activation energy, International Communications in Heat and Mass Transfer, Vol. 112, 104401.

Xu, Q. (2016). Development of Advanced Creep Damage Constitutive Equations for Low CR Alloy Under Long Term Service, PhD thesis, The University of Huddersfield.

Yoon, H.K. and Ghajar, A.J. (1987). A note on the Powell-Eyring fluid model, Int. Comm. Heat Mass Transfer, Vol. 14, pp. 381–390.

Zhavoronkov, N.M., Malyusov, V.A., Mochalova, N.S. and Kholpanov, L.P. (1978). Mass transfer in a liquid layer of variable thickness on a rotating Archimedes spiral taking account of the entrance region, Zhurnal Prikladuoi Mekhaniki I Tekhnicheskoi Fiziki.

Zin, N.A.M., Khan, I., Shafie, S. and Alshomrani, A.S. (2017). Analysis of heat transfer for unsteady MHD free convection flow of rotating Jeffrey nanofluid saturated in a porous medium, Results in Physics, Vol. 7, pp. 288–309.